ITRF2008 plate motion model

Z. Altamimi, Laurent Métivier, X. Collilieux

ITRF2008 plate motion model

Z. Altamimi,[1] L. Métivier,[1,2] and X. Collilieux[1]

Received 11 October 2011; revised 22 May 2012; accepted 23 May 2012; published 4 July 2012.

[1] The ITRF2008 velocity field is demonstrated to be of higher quality and more precise than past ITRF solutions. We estimated an absolute tectonic plate motion model made up of 14 major plates, using velocities of 206 sites of high geodetic quality (far from plate boundaries, deformation zones and Glacial Isostatic Adjustment (GIA) regions), derived from and consistent with ITRF2008. The precision of the estimated model is evaluated to be at the level of 0.3 mm/a WRMS. No GIA corrections were applied to site velocities prior to estimating plate rotation poles, as our selected sites are outside the Fennoscandia regions where the GIA models we tested are performing reasonably well, and far from GIA areas where the models would degrade the fit (Antarctica and North America). Our selected velocity field has small origin rate bias components following the three axis (X, Y, Z), respectively 0.41 ± 0.54, 0.22 ± 0.64 and 0.41 ± 0.60 (95 per cent confidence limits). Comparing our model to NNR-NUVEL-1A and the newly available NNR-MORVEL56, we found better agreement with NNR-MORVEL56 than with NNR-NUVEL-1A for all plates, except for Australia where we observe an average residual rotation rate of 4 mm/a. Using our selection of sites, we found large global X-rotation rates between the two models (0.016°/Ma) and between our model and NNR-MORVEL56 of 0.023°/Ma, equivalent to 2.5 mm/a at the Earth surface.

Citation: Altamimi, Z., L. Métivier, and X. Collilieux (2012), ITRF2008 plate motion model, *J. Geophys. Res.*, *117*, B07402, doi:10.1029/2011JB008930.

1. Introduction

[2] Before long time-span geodetic observations were collected, tectonic plate motion models were constructed using only geological and geophysical data. The first global plate motion models were available in the early 70's; e.g. the derived absolute model AM02 from *Minster and Jordan* [1978] was, for example, recommended to the users of the International Terrestrial Reference Frame (ITRF), until the time when a first ITRF velocity field was estimated using space geodesy results [*Altamimi et al.*, 1993]. At that time, the No-Net-Rotation (NNR) concept was adopted to define the ITRF orientation time evolution. This condition is implicitly satisfied by initial rotational alignment of the ITRF velocity field to the available geophysical models, and then by successive alignments of ITRF solutions with each other. For instance, ITRF2000 was aligned with NNR-NUVEL-1A (abbreviated hereafter by NNR1A) [*Argus and Gordon*, 1991; *DeMets et al.*, 1990, 1994], ITRF2005 to ITRF2000, and ITRF2008 to ITRF2005 [*Altamimi et al.*, 2002, 2007, 2011]. For further details regarding the frame specifications of the ITRF solutions, the reader may refer to Chapter 4 of the IERS Conventions [*Petit and Luzum*, 2010].

[3] Despite the relatively sparse geodetic networks, which will never discretize the entire Earth's surface, attempts were however made to construct NNR frames, using space geodesy results [*Drewes*, 1998; *Kreemer et al.*, 2006; *Legrand*, 2007]. However, *Altamimi et al.* [2003, 2007] concluded that the uncertainty of ITRF NNR condition implementation was at the level of 2 mm/a, which is still the case today, as it will be shown here in comparison with the newly released NNR-MORVEL56 (abbreviated hereafter by NNRM56) [*Argus et al.*, 2011a], based on the MORVEL relative model [*DeMets et al.*, 2010].

[4] The ITRF2008 velocity field is demonstrated to be of higher quality and more precise than past ITRF solutions [*Altamimi et al.*, 2011]. For various geodetic and geophysical applications of ITRF2008, the aim of this paper is to provide users with the most precise plate motion model derived from and consistent with the ITRF2008. Section 2 recalls the procedure used for the estimation of plate angular velocities and describes the criteria adopted for site selection. Section 3 discusses the impact of GIA on plate motion estimation, and section 4 discusses the uncertainty of the frame origin rate. In section 5, we present our ITRF2008 plate motion model (ITRF2008-PMM) and we compare it with the GEODVEL model of *Argus et al.* [2010]. In section 6, we quantify the

[1]Laboratoire de Recherche en Géodésie, Institut National de l'Information Géographique et Forestière, Champs-sur-Marne, France.
[2]Institut de Physique du Globe de Paris, Paris, France.

Corresponding author: Z. Altamimi, Laboratoire de Recherche en Géodésie, Institut National de l'Information Géographique et Forestière, 6 & 8 Avenue Blaise Pascal, FR-77455 Champs-sur-Marne, France. (zuheir.altamimi@ign.fr)

0148-0227/12/2011JB008930

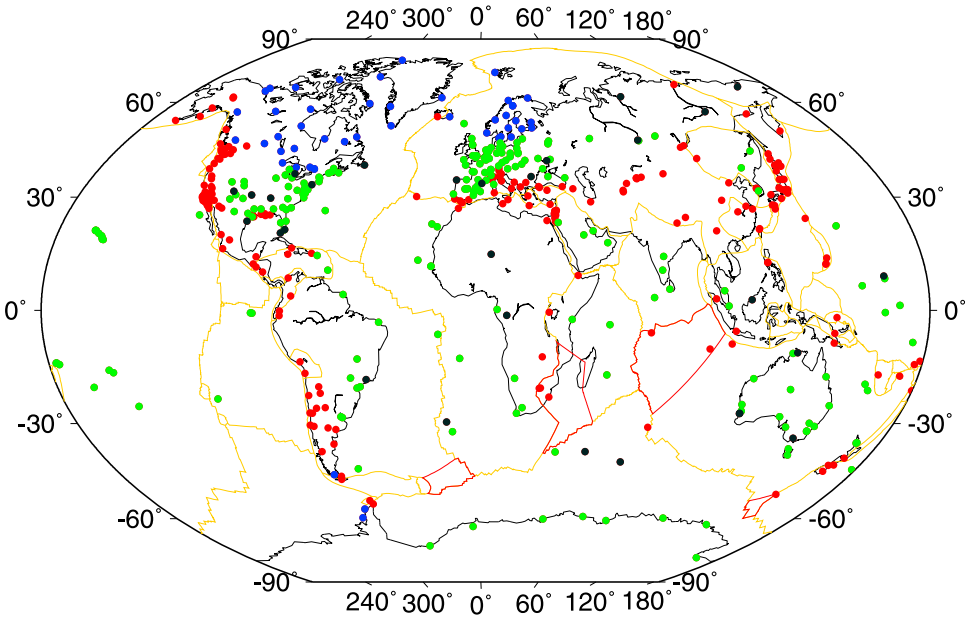

Figure 1. ITRF2008 sites with time-span longer than three years. Red: sites close to plate boundaries or in deformation zones. Blue: sites located in GIA regions. Black: sites with normalized velocity residuals larger than 3, or raw residuals larger than 3 mm/a. Green: our final selection of 206 sites. *Bird*'s [2003] plate boundaries are shown in orange, and the four additional MORVEL plates in red [*DeMets et al.*, 2010].

consistency between ITRF2008 and the two geological models (NNR1A and NNRM56) and evaluate the uncertainty of the ITRF2008 NNR condition implicit realization.

2. Estimation of Plate Angular Velocities and Site Selection

2.1. Inversion Model

[5] The basic equation used for the estimation of plate angular velocities links the Euler vector ω_p with point velocity $\dot{X}_i$, of position vector X_i, located on plate p:

$$\dot{X}_i = \omega_p \times X_i. \tag{1}$$

[6] When estimating all plate angular velocities together from a global velocity field, we can add an origin rate component to equation (1) [*Argus et al.*, 2010] so that

$$\dot{X}_i = \omega_p \times X_i + \dot{T} \tag{2}$$

where $\dot{X}_i$ represents the ITRF2008 input horizontal site velocities and $\dot{T}$ is the origin translational vector of the implied velocity filed. $\dot{T}$ could be regarded as an origin rate bias (ORB) of the velocity field materialized by the selected sites. In the following, we use equation (2) as our inversion model and provide detailed discussion about the relevance of the ORB in section 4.

[7] There are several ways to estimate plate angular velocities, either individually or in a global inversion involving all plates, using the inverse of the full variance-covariance matrix or diagonal terms as weighting. We used full variance-covariance matrix in our simultaneous inversions of all plates, together with the ORB, in order to reflect more realistic formal errors.

[8] The uncertainties of the estimated parameters listed in all tables of this paper (except Table A1 in Appendix A where we listed the original ITRF2008 formal errors) are one-sigma formal errors as a result of the least squares adjustment. They were normalized (multiplied) by the square root of the Variance Factor (VF) of unit weight given by

$$VF = \frac{v^T P v}{f} \tag{3}$$

where v is the vector of post fit residual site velocities, P is the weight matrix (the inverse of the variance-covariance matrix). f is the number of degrees of freedom of the least squares adjustment, which is equal to the difference between the number of observations and the number of unknowns.

[9] The VF is a function of the a priori uncertainties of site velocities which are heterogeneous. Indeed, these a priori velocity uncertainties are the formal errors resulting from the original ITRF2008 adjustment, which are function of the time-span of the observations of each site. The time-span of our selected sites ranges from 3.2 up to 29 years.

2.2. Site Selection

[10] An important aspect to be taken into account is the selection of points within each plate. Indeed, site selection should account for geophysical and geodetic considerations, e.g. plate boundaries and intraplate deformation zones, site distribution, reliability of site velocities. The magnitude of the post-fit residuals could be an indicator of, e.g. the local motion or unknown instrumental systematic errors. For the search of the most precise estimation of an ITRF2008-PMM, we elaborated a large number of estimation tests and ended up by selecting ITRF2008 sites satisfying the following three

Table 1. Eurasia Plate Rotation Poles With and Without GIA Corrections

Plate	NS[a]	ω_x (mas/a)	ω_y (mas/a)	ω_z (mas/a)	ω (°/Ma)	WRMS[b] E	WRMS[b] N
			EURA: No GIA Correction				
EURA	90	−0.081 ± 0.010	−0.524 ± 0.010	0.755 ± 0.007	0.256 ± 0.002	0.45	0.49
			EURA: With VM2 Model Corrections				
EURA	90	−0.075 ± 0.008	−0.515 ± 0.008	0.755 ± 0.006	0.255 ± 0.002	0.48	0.42
			EURA: With VM4 Model Corrections				
EURA	90	−0.073 ± 0.008	−0.521 ± 0.009	0.760 ± 0.006	0.257 ± 0.002	0.50	0.41
			EURA: With SV Model Corrections				
EURA	90	−0.088 ± 0.008	−0.512 ± 0.008	0.756 ± 0.006	0.255 ± 0.002	0.40	0.36
			EURA: No GIA Correction				
EURA	69	−0.085 ± 0.006	−0.530 ± 0.007	0.751 ± 0.005	0.256 ± 0.002	0.39	0.29
			EURA: With VM2 Model Corrections				
EURA	69	−0.081 ± 0.007	−0.519 ± 0.008	0.749 ± 0.006	0.254 ± 0.002	0.48	0.34
			EURA: With VM4 Model Corrections				
EURA	69	−0.087 ± 0.007	−0.527 ± 0.008	0.746 ± 0.006	0.255 ± 0.002	0.46	0.29
			EURA: With SV Model Corrections				
EURA	69	−0.089 ± 0.006	−0.515 ± 0.007	0.759 ± 0.005	0.256 ± 0.002	0.36	0.30

[a]Number of sites.
[b]Weighted root mean scatter in east and north in mm/a.

main criteria: (1) the time-span of observations per site had to be longer than three years, (2) the sites were to be at least 100 km from *Bird* [2003] plate boundaries, outside deformation areas following the criteria of *Argus and Gordon* [1996] and the strain map of *Kreemer et al.* [2003, 2006], and far from GIA regions (see discussion in section 3), and (3) the normalized post-fit velocity residuals (raw residuals divided by their a priori uncertainties) are smaller than 3 and the raw residuals are less than 3 mm/a (abbreviated hereafter by 3-sigma-3 mm). While condition 1 is imposed to avoid using biased station velocities by possible seasonal signals [*Blewitt and Lavallée*, 2002], condition 2 would be a necessary requirement to satisfy rigid plate motion theory. The threshold of three-sigma normalized residuals is commonly used in least squares adjustment allowing to detect and reject data outliers. Condition 3 is operated iteratively, using our adopted inversion model (equation (2)): the inversion is repeated until convergence, where no more site velocity residuals are larger than 3-sigma-3 mm. We verified that the few rejected sites (9) with raw velocity residuals larger than 3 mm/a have no impact on our results. They were actually rejected after the first run.

[11] Figure 1 illustrates four classes of site selection with different colors. 509 sites satisfy condition 1, 227 sites (red points in Figure 1) are close to plate boundaries or located in deformation zones. 20 of the 227 sites were identified by D. Argus (personal communication, 2012) to be located close to plate boundaries, active faults, large earthquakes, and/or tectonic topography that mark plate boundaries, following the criteria of *Argus and Gordon* [1996]. 47 sites (blue points) are located in GIA regions (see Section 3) and 29 sites (black points) with velocity residuals larger than 3-sigma-3 mm. Our final adopted velocity field that satisfies all three conditions is made up of 206 sites (green points in Figure 1), where 55% of them are located in North America (44 sites) and Eurasia (69 sites). Note that the time-span of data used to estimate the site velocities is longer than 7 years for 80% of the selected sites, whereas 90% have a formal error less than 0.12 mm/a.

3. Plate Motion and Glacial Isostatic Adjustment

[12] The linear velocities resulting from the ITRF combination are impacted by GIA in areas where this phenomenon occurs. Antarctica (ANTA), Eurasia (EURA) and North America (NOAM) are the plates known to be most affected by GIA. Correcting the linear velocities by applying a GIA model before rotation pole estimation may reflect more appropriately tectonic motions, provided that the model used is precise enough in describing GIA horizontal displacement [*Plag et al.*, 2002; *Kierulf et al.*, 2003].

[13] We attempted to use GIA models ICE-5G/VM2 and VM4 from *Peltier* [2004] and another one from *Schotman and Vermeersen* [2005] (named hereafter VM2, VM4 and SV, respectively) over the three aforementioned plates, by subtracting the model predictions from the linear horizontal velocities. These three GIA models are the only models providing horizontal velocities that are publicly available at the Website of the Special Bureau for Loading [*van Dam et al.*, 2002]. We observed that the magnitude of predicted horizontal velocities in the SV model for our selected sites is less than 1 mm/a for the three considered plates. While VM2 and VM4 models predict velocities less than 1 mm/a in EURA and ANTA, their prediction in NOAM is much larger, reaching up to 3 mm/a.

[14] As an example, Table 1 lists the angular velocity components for Eurasia plate with and without GIA model corrections, together with the Weighted Root Mean Scatter (WRMS) of each estimation. In these estimations we used equation (1), i.e. without the translation rate vector. When

using the full set of Eurasia sites (90), including sites in Fennoscandia regions, applying VM2 or VM4 model corrections improves the fit in the north component only: the north WRMS decreases by 0.07 and 0.08 mm/a, respectively. Applying SV model corrections decreases the WRMS in both east and north by 0.05 and 0.13 mm/a, respectively. However, when using the 69 Eurasia sites extracted from our final selection, applying VM2 or VM4 GIA model corrections degrades the fit, while SV model improves the fit only marginally (see Table 1). Indeed our selection excludes all sites located in Fennoscandia where the GIA effect is the most significant. These results suggest that the GIA models are performing reasonably well in Fennoscandia region, while their predictions in the other parts of Europe are marginal and have no effect on Eurasia angular velocity.

[15] We also tested the three models over ANTA and NOAM sites. For ANTA, correcting the nine involved site velocities by VM2 or VM4 predictions improves the fit in the north component by 0.10 mm/a, while the east component is degraded by 0.06 mm/a RMS. SV model performs less effectively than the VM2 or VM4: the fit is degraded by respectively 0.15 and 0.29 mm/a RMS in the east and north components. For NOAM, applying VM2 or VM4 model corrections degrades the results significantly (up to 1 mm/a in both components), as already noted by *Argus and Peltier* [2010]. SV model improves the fit very slightly by 0.02 mm/a WRMS in the north component only, and only when all NOAM sites (88) are used.

[16] From the above tests we conclude that we would be able to estimate a precise plate motion model without applying any GIA model predictions. The only condition is to avoid including sites in GIA areas in our final site selection, as also applied by *Argus et al.* [2010]. Towards this end, we identified 47 sites located in GIA regions following *Paulson et al.*'s [2007] model, which is similar to *Peltier*'s [2004] classical model, but with a smaller rotational feedback impact (see *Chambers et al.* [2010] or *Métivier et al.* [2012] for a discussion about the relevance of this model). We assigned a site to GIA category if its modeled vertical velocity is larger than 0.75 mm/a. We did not take into account GIA horizontal velocity predictions in our selection, given the results of our own analysis as discussed above, and because it has been shown that they tend to be strongly overestimated compared with geodetic data in North America [*Argus and Peltier*, 2010].

4. ITRF2008-PMM and the Frame Origin

[17] An ITRF origin drift would have serious consequences in Earth science studies such as sea level variability and GIA [*King et al.*, 2010; *Collilieux and Woppelmann*, 2010]. It is therefore legitimate to question how accurate the ITRF2008 origin is and whether it has significant drift over time. Let us recall that there is a Z-translation rate of 1.8 mm/a from ITRF2000 to ITRF2005 and that component is zero between ITRF2005 and ITRF2008 [*Altamimi et al.*, 2007, 2011]. Such a Z-translation rate ($\dot{T}_Z$) has an impact on the north velocity component and is equal to $\dot{T}_Z \times \cos(\phi)$, where ϕ is the latitude. Therefore a frame origin drift may influence the estimation of plate angular velocities.

[18] The translation rate $\dot{T}$ in equation (2) has been suggested by *Argus* [2007]. He has interpreted it as the linear displacement between the estimate of the Center of Mass (CM) from SLR observations and the estimate of the center of mass of the solid Earth (CE) from site velocities on the Earth's surface. He furthermore argues that the velocity between CM and CE is negligible. Although they used an identical equation, *Kogan and Steblov* [2008] proposed another origin name for the above definition and introduced the Center of Plate motion (CP). As we are dealing with surface site velocities, and that Euler poles refer to geometric deformations, we think that plate angular velocities are estimated with respect to the Center of Figure (CF) of the solid Earth, see *Blewitt* [2003] for CF definition. However, the origin of the $\dot{T}$ vector may not be exactly the CM, that's why we suggested the term ORB here. As a consequence, the negative of the ORB, (i.e. $-\dot{T}$), introduced in our inversion model (equation (2)) could be interpreted as the sum of an origin drift error of the reference frame materialized by the selected sites and the geocenter velocity (CM with respect to CF).

[19] *Kogan and Steblov* [2008] and *Argus et al.* [2010] estimated an ORB together with plate angular velocities and found different values for the $\dot{T}_Z$ with respect to ITRF2005 origin: 2.5 versus 1.2 mm/a, respectively. The difference of 1.3 mm/a between the two estimates is most likely to be due, partly, to the selection of sites used and their distribution over the plates, as it will be illustrated latter. Another approach used by *Argus et al.* [2010] consists in combining GIA predicted vertical velocities and horizontal velocities from space geodesy to estimate both an ORB and plate angular velocities. They found a $\dot{T}_Z$ between 0.1 and 1.1 mm/a with respect to ITRF2005, depending on the GIA model used. Using multiple geodetic data sets (combining 233 tri-dimensional (3-D) ITRF2008 site velocities with GRACE gravity and Ocean Bottom Pressure (OBP) models) and a simultaneous global inversion approach, *Wu et al.* [2011] estimated additional parameters to model GIA effect and Present Day Mass Trends (PDMT). They separated the origin drift error and geocenter velocity and found respectively -0.5 mm/a and -0.8 mm/a (for both GIA and PDMT) [*Wu et al.*, 2011; X. Wu, personal communication, 2012] equivalent to 1.3 mm/a in total for $\dot{T}_Z$. However, we note that the first value depends on OBP and GRACE data and the second is in the upper limit of other published values [*Greff-Lefftz et al.*, 2010; *Métivier et al.*, 2010]. As a consequence, we prefer estimating in the following our own ORB as an independent study.

[20] After rejecting sites close to plate boundaries, in deformation zones and GIA regions, we were left with 235 sites (the sum of dark and green sites shown in Figure 1). We then operated an iterative process of our inversion to reject outliers using equation (2) as presented in section 2.2, ending up with the 206 green sites shown in Figure 1. The obtained three components of the ORB are listed in Table 2, together with their one-sigma formal errors. The estimated ORB could be considered as not significant at the 95 per cent confidence level (i.e. two-sigma confidence level).

[21] Our results differ from previous studies that also used equation (2). Our selected velocity field of 206 sites cannot represent the entire frame of the ITRF2008 composed of

Table 2. Translation Rate Components

Number of Sites					
Total	EURA	NOAM	$\dot{T}_x$ (mm/a)	$\dot{T}_y$ (mm/a)	$\dot{T}_z$ (mm/a)
206	69	44	0.41 ± 0.27	0.22 ± 0.32	0.41 ± 0.30

580 sites. In fact, another selection of ITRF2008 site velocities would produce different ORB results. Indeed, *Argus et al.* [2011b, Figure S3] have used a sub-set of ITRF2008 site velocities and found 1.2 mm/a for the $\dot{T}_z$ component. The relatively large difference with our estimate is most likely to be due to differences in the selection of sites and their distribution over the plates. Indeed, we selected a velocity field made up of 124 sites used by *Argus et al.* [2010] to determine plate angular velocities. Applying our iterative procedure, 8 of the 124 sites were rejected, their normalized residuals being larger than three-sigma. Using the remaining 116 sites, we found a Z-translation rate of 0.99 (±0.23) mm/a, consistent with *Argus et al.* [2011b]. However, rejecting only two sites (Kerguelen Island, and Norilsk, Russia), which have actually been rejected from our initial set of 235 sites during our iterative process (their normalized residuals being larger than three-sigma), the Z-translation rate dropped to 0.42 (±0.25) mm/a.

[22] Our Z-translation rate ($\dot{T}_z$) is one third of the estimate of *Argus et al.* [2010], and smaller than the estimate of *Wu et al.* [2011] by 0.9 mm/a. It is likely that the addition of GRACE and OBP data and an extended modeling make the results of *Wu et al.* [2011] less sensitive to the network of sites used, but this would need further evaluation. But if we assume as *Argus* [2007] that the vector $\dot{T}$ is the velocity of CE in the ITRF, instead of the velocity of CF as we did here, the equivalent $\dot{T}_z$ from *Wu et al.* [2011] would be 0.7 mm/yr since only PDMT contribute to the current motion of CE with respect to CM, in addition to the ITRF2008 origin rate error they estimated. In this case our estimate of $\dot{T}_z$ would be smaller than the estimate of *Wu et al.* [2011] by 0.2 mm/a. However, the extended study by *Wu et al.* [2011] used 3-D site velocities as input (including sites in GIA regions), while with equation (2) we used only horizontal site velocities. Therefore *Wu et al.* [2011] values and ours cannot be compared. Our $\dot{T}$ would therefore contain the contribution of only horizontal site velocities to the geocenter velocity estimation and would probably reflect an incomplete estimation of the geocenter velocity. However, we focus here on plate motion models only, and further studies are still needed to confirm the estimation of the geocenter velocity from *Wu et al.* [2011]. As we observe no systematic pattern in our site velocity residuals, we prefer considering our estimate as a reference for discussion in the next section.

5. ITRF2008 Plate Motion Model

[23] Considering the results of the GIA impact investigation discussed in section 3, we adopted the option of not correcting the site velocities by any GIA model predictions, and rejecting the 47 sites located within GIA regions. The introduction of a translation rate vector in equation (2), allows quantifying the ORB and its impact on the estimated plate angular velocities. Adopting an outlier threshold based on the normalized three-sigma velocity residuals leaded to a velocity field that has a small ORB, which could be considered as insignificant. However, our ITRF2008-PMM is derived with equation (2), i.e. with estimating the translation rate parameter, and using the 206 sites that satisfy the three main criteria for a robust plate motion estimation.

5.1. Estimated Plate Angular Velocities

[24] Table 3 lists the angular velocities adopted for the 14 plates of the ITRF2008-PMM, where the global WRMS of the fit are respectively 0.33 and 0.31 mm/a in east and north component. In addition to ANTA, EURA and NOAM, the plates listed in Table 3 by their abbreviations are: Amurian (AMUR), Arabia (ARAB), Australia (AUST), Caribbean (CARB), India (INDI), Nazca (NAZC), Nubia (NUBI), Pacific (PCFC), S. America (SOAM), Somalia (SOMA) and Sundaland (SUND). Table A1 in Appendix A lists the 206 selected sites and their horizontal velocities, together with one sigma formal errors and their post-fit residuals. It also lists the 29 rejected sites where the velocity residuals exceed the threshold of 3-sigma-3 mm.

[25] The angular velocities of five plates were determined with three to four sites, and two plates with two sites only,

Table 3. ITRF2008 Absolute Plate Rotation Poles

Plate	NS[a]	ω_x (mas/a)	ω_y (mas/a)	ω_z (mas/a)	ω (°/Ma)	WRMS E	WRMS N
AMUR	3	−0.190 ± 0.040	−0.442 ± 0.051	0.915 ± 0.049	0.287 ± 0.008	0.14	0.24
ANTA	9	−0.252 ± 0.008	−0.302 ± 0.006	0.643 ± 0.009	0.209 ± 0.003	0.40	0.29
ARAB	4	1.202 ± 0.082	−0.054 ± 0.100	1.485 ± 0.063	0.531 ± 0.027	0.23	0.15
AUST	19	1.504 ± 0.007	1.172 ± 0.007	1.228 ± 0.007	0.630 ± 0.002	0.29	0.25
CARB	2	0.049 ± 0.201	−1.088 ± 0.417	0.664 ± 0.146	0.354 ± 0.122	0.06	0.04
EURA	69	−0.083 ± 0.008	−0.534 ± 0.007	0.750 ± 0.008	0.257 ± 0.002	0.34	0.28
INDI	4	1.232 ± 0.031	0.303 ± 0.128	1.540 ± 0.030	0.554 ± 0.017	0.55	0.55
NAZC	3	−0.330 ± 0.011	−1.551 ± 0.029	1.625 ± 0.013	0.631 ± 0.005	0.09	0.08
NOAM	44	0.035 ± 0.008	−0.662 ± 0.009	−0.100 ± 0.008	0.186 ± 0.002	0.27	0.32
NUBI	11	0.095 ± 0.009	−0.598 ± 0.007	0.723 ± 0.009	0.262 ± 0.003	0.26	0.35
PCFC	23	−0.411 ± 0.007	1.036 ± 0.007	−2.166 ± 0.009	0.677 ± 0.002	0.42	0.44
SOAM	10	−0.243 ± 0.009	−0.311 ± 0.010	−0.154 ± 0.009	0.118 ± 0.002	0.44	0.34
SOMA	3	−0.080 ± 0.028	−0.745 ± 0.030	0.897 ± 0.012	0.325 ± 0.007	0.28	0.21
SUND	2	0.047 ± 0.381	−1.000 ± 1.570	0.975 ± 0.045	0.388 ± 0.308	0.08	0.05
ITRF2008-PMM						0.33	0.31

[a]Number of sites.

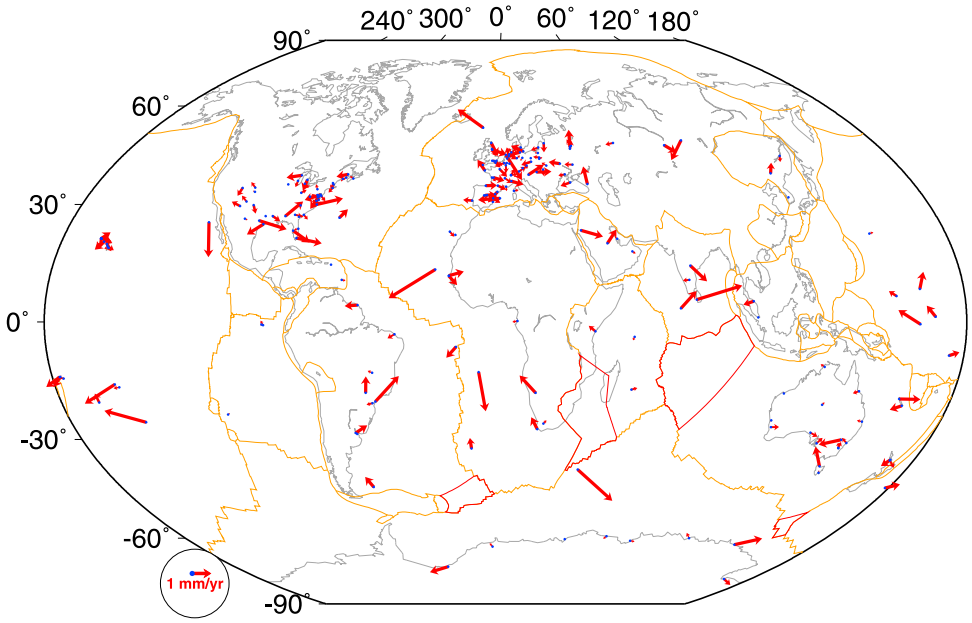

Figure 2. Geographic distribution of ITRF2008-PMM site velocity residuals.

see Table 3. The WRMS of the fit per plate ranges from 0.1 to 0.6 mm/a, the largest being for INDI plate, and so its estimated rotation pole is probably the weakest among the 14 plates.

[26] Figure 2 illustrates the geographic distribution of the ITRF2008-PMM site velocity residuals. Inspecting this figure, we can see that there is no systematic behavior for any of the 14 plates.

[27] The users of ITRF2008-PMM are advised to apply not only plate angular velocities listed in Table 3, but also the translation rate components of Table 2.

5.2. Comparison Between ITRF2008-PMM and GEODVEL

[28] It is worth comparing ITRF2008-PMM results to other models derived from space geodesy data. *Argus et al.* [2010] derived GEODVEL model by simultaneously estimating the angular velocities of 11 major plates together with the origin translation rate components, combining individual solutions from the four techniques (VLBI, SLR, GPS, DORIS). We compared GEODVEL model to ITRF2008-PMM, by differentiating their predicted site velocities, using their respective plate angular velocities, as

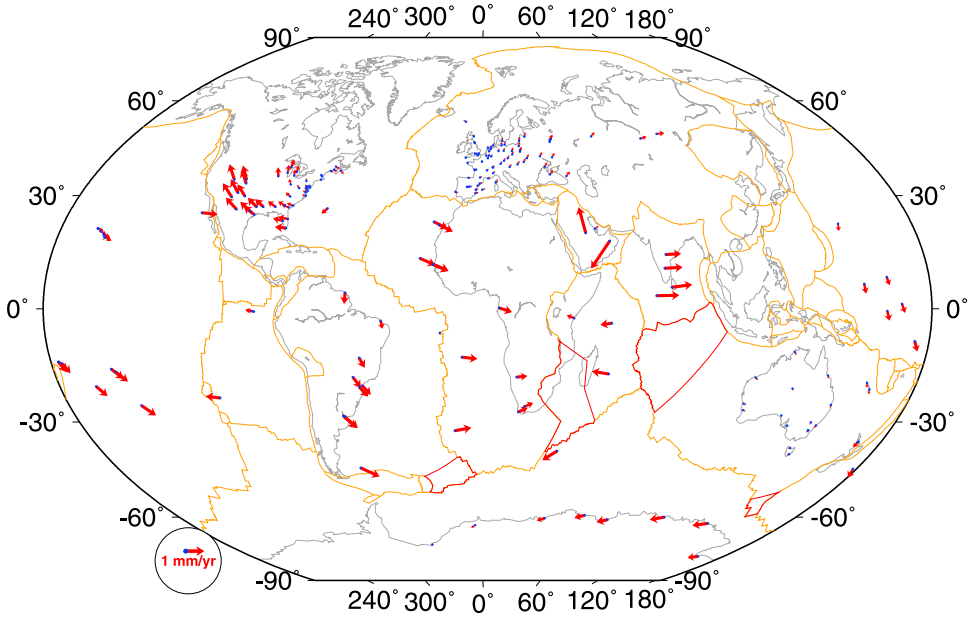

Figure 3. Differences between predicted site velocities by ITRF2008-PMM and GEODVEL [*Argus et al.*, 2010].

Table 4. Rotation Rate Components and RMS Between NNR1A, NNRM56 and ITRF2008

From	To	NS	NP[a]	$\dot{R}_x$ (mas/a)	$\dot{R}_y$ (mas/a)	$\dot{R}_z$ (mas/a)	RMS E	RMS N
NNR1A	NNRM56	198	11		no transformation		2.1	1.4
NNR1A	NNRM56	165	7	0.058 ± 0.002	-0.008 ± 0.001	-0.026 ± 0.002	0.9	0.7
		198	11		as above		2.0	1.3
ITRF2008	NNR1A	198	11		no transformation		2.4	2.0
ITRF2008	NNR1A	133	7	-0.003 ± 0.002	0.023 ± 0.002	-0.010 ± 0.002	0.8	1.1
		198	11		as above		2.5	2.1
ITRF2008	NNRM56	206	14		no transformation		2.0	2.2
ITRF2008	NNRM56	143	10	0.083 ± 0.002	0.006 ± 0.002	-0.007 ± 0.002	1.0	1.1
		206	14		as above		1.8	1.9

[a]Number of plates.

well as their translation rate components. In this comparison, we used GEODVEL angular velocities rotationally aligned to ITRF2005 to predict velocities for 198 sites, to which we also applied the translation rate components as provided by D. Argus (personal communication, 2012). The 198 sites are extracted from our final selection of 206 sites, located at the 11 plates of *Argus et al.* [2010]. We verified that there is insignificant rotation rate between the two models, as expected, given the fact that the ITRF2008 is rotationally aligned to ITRF2005. Figure 3 illustrates the 198 site velocity differences between GEODVEL and ITRF2008-PMM predictions. Inspecting that figure, we can see that there are insignificant differences for AUST and EURA sites, differences up to 0.4 mm/a for the majority of sites and larger than 1 mm/a for some others. The RMS of these differences is 0.4 mm/a, in both east and north components, indicating the level of agreement between the two models.

6. Comparisons to Geological Models

[29] From the point of view of the ITRF2008's implicit rotational alignment to NNR-NUVEL-1A, the availability of the new NNR-MORVEL56 raises the question whether the latter could be used in future ITRF solutions. Indeed, NNR-MORVEL56 is believed to be superior to (and samples more plates than) NNR-NUVEL-1A [*Argus et al.*, 2011a]. Therefore, their mutual comparison first (independently from ITRF2008 data), and then with ITRF2008 is an important procedure in the analysis to help answer that question. It is obviously beyond the scope of this paper to compare the two geological relative models. A thorough and comprehensive comparison between them is extensively provided by *DeMets et al.* [2010].

[30] We used the 206 selected sites for our ITRF2008-PMM as a basis for comparison, quantifying the level of consistency between NNR1A, NNRM56 and ITRF2008, as well as the NNR condition uncertainty evaluation. Since the two geological models average the horizontal plate motion over the entire sphere, we estimated three rotation rates between the three associated velocity fields. The rotation rates (estimated by un-weighted least squares adjustment) and RMS values resulting from the different comparisons which we operated are listed in Table 4. In order to obtain estimated rotation rates with a precision of or better than 1 mm/a RMS, in the three cases listed in Table 4, we retained sites where the post-fit residuals are less than 3 mm/a.

[31] The results of the comparisons presented below are to be taken with some caution. Indeed, the time scale over which geological models average plate motion (between 0.78 and 3.16 Ma for MORVEL, and 3.16 Ma for NUVEL-1A [*DeMets et al.*, 2010]) may not represent the current motion of possible slowing or speeding plates as sensed by space geodesy.

6.1. Comparison Between NNR-NUVEL-1A and NNR-MORVEL56

[32] We compared NNR1A and NNRM56 by first differentiating their predicted velocities for 198 sites located on 11 plates that are common to the two models and are part of our selected sites. As listed in Table 4, the RMS of these velocity differences are respectively 2.1 and 1.4 mm/a in east and north components. The 198 site velocity differences are illustrated in Figure 4 (left) where we can see that the largest velocity differences are for sites located on ARAB, CARB, INDI and NAZC plates.

[33] As we could have expected using one of these two models to define the ITRF2008 orientation rate, it is relevant to test if they differ by a rotation rate over our selected network.

[34] We then estimated three rotation rates between the two geological models using 165 sites (located on 7 plates) satisfying the post-fit residual threshold of 3 mm/a. As listed in Table 4, we found a large rotation rate around the X-axis of 0.058 mas/a between the two models, equivalent to 1.8 mm/a at the Earth surface, with RMS of the fit smaller than 1 mm/a over the two components. The site velocity residuals, after removing the estimated rotation rate from the entire 198 site velocities, are illustrated in Figure 4 (right), and the corresponding RMS are respectively 2.0 and 1.3 mm/a in east and north components. It is worth noting that the two models agree better in the north than in the east component. From this figure we can see that while the estimated rotation rate attenuates the velocity differences between the two models for sites on EURA, NOAM, NUBI, SOAM, and partly for sites on PCFC and ANTA plates, all the AUST site residual velocities are amplified by at least 1 mm/a, reaching up to 4.6 mm/a. According to *Argus et al.* [2011a] (Table 4), the AUST velocity difference between NNRM56 and NNR1A is 0.046°/Ma, which is equivalent to approximately 5 mm/a. Therefore the rotation rate of 1.8 mm/a that we estimated between the two models, at the level of 0.9 and 0.7 mm/a RMS in east and north components, does not, and cannot accommodate the large AUST

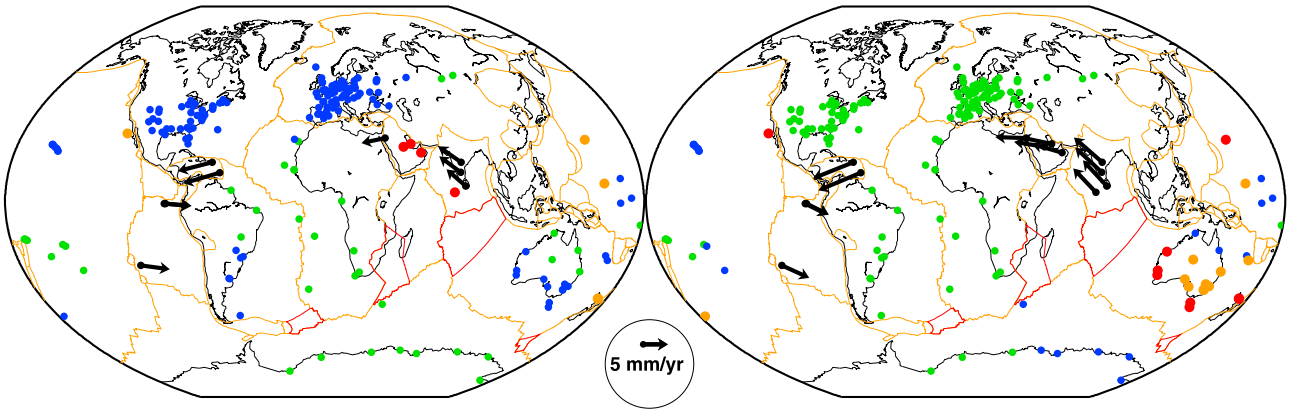

Figure 4. Velocity differences between NNR-NUVEL-1A and NNR-MORVEL56 (velocities of the latter are subtracted from the former): (left) raw and (right) after rotation rate transformation. Green: less than 2 mm/a. Blue: between 2–3 mm/a. Orange: between 3–4 mm/a. Red: between 4–5 mm/a. Black: larger than 5 mm/a, and rates of velocity differences are shown only in this case.

site velocity differences between the two models. This behavior might be caused by the fact that AUST plate is only connected to MORVEL via ANTA plate, according to the MORVEL plate circuit [*DeMets et al.*, 2010, Figure 2].

6.2. Comparison Between ITRF2008 and Geological Models

[35] We compared ITRF2008 with the two models, by differentiating their raw velocities, involving 198 sites for NNR1A and the full set of our selected sites (206) for NNRM56, as illustrated in Figure 5. The analyzed sites considered here are those located on common plates between ITRF2008 and each model. Indeed, there are 8 sites located on 3 plates (AMUR, SUND and SOMA) included in NNRM56 and not in NNR1A. The RMS of these differences are, in east and north components, 2.4 and 2.0 mm/a for NNR1A, 2.0 and 2.2 mm/a for NNRM56. As it can be seen from Figure 5 (left), the largest RMS values for NNR1A are due to the large differences with ITRF2008 velocities for sites located on ARAB, CARB, INDI and NAZC plates, for which we notice better agreement between ITRF2008 and NNRM56. In the case of the comparison between the ITRF2008 and NNRM56, the larger RMS values are mainly due to a large rotation rate between the two (see discussion below).

[36] We then adjusted three rotation rates between ITRF2008 and each geological model, rejecting, iteratively, these sites with post-fit residuals larger than 3 mm/a. 133 sites located on 7 plates were used for NNR1A and 143 sites located on 10 plates for NNRM56. Note that only two PCFC sites (located on Chatham Island and Isla Guadalupe) have been included in the ITRF2008 and NNR1A rotation rate fit that have post-fit residuals less than 3 mm/a. Only two AUST sites (TAKL, Auckland and KOUC, New Caledonia) have been included in the ITRF2008 and NNRM56 rotation rate fit. The RMS of these two transformations are, in east and north components, 0.8, 1.1 for NNR1A and 1.0, 1.1 mm/a for NNRM56.

[37] The small rotation rates found between ITRF2008 and NNR1A show that the implicit alignment of ITRF2008 to NNR1A is quite satisfied, at the level of or better than 1 mm/a. Indeed, the largest velocity difference induced by the estimated rotation rate is 0.9 mm/a at the Earth surface. However, removing the estimated three rotation rates from

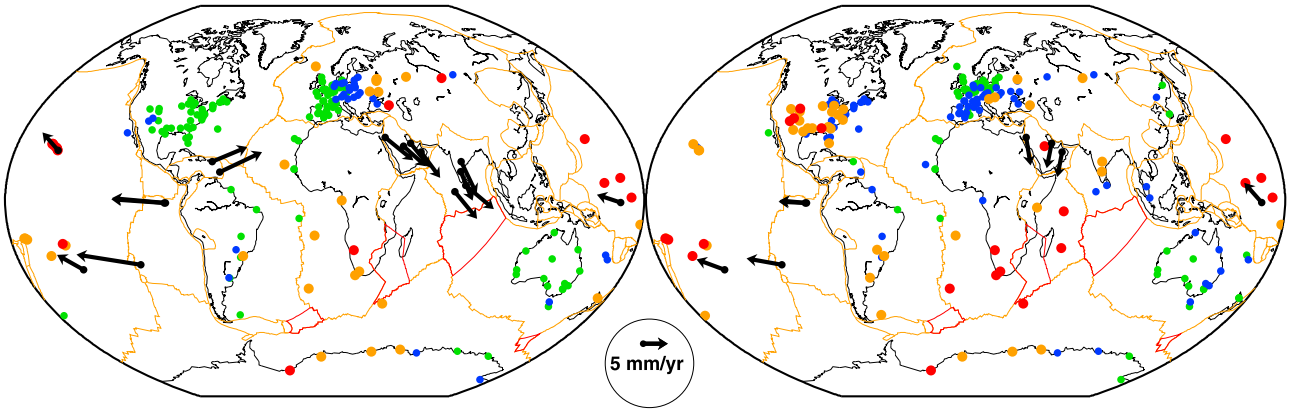

Figure 5. Raw velocity differences between ITRF2008 and (left) NNR-NUVEL-1A and (right) NNR-MORVEL56. Legend as in Figure 4.

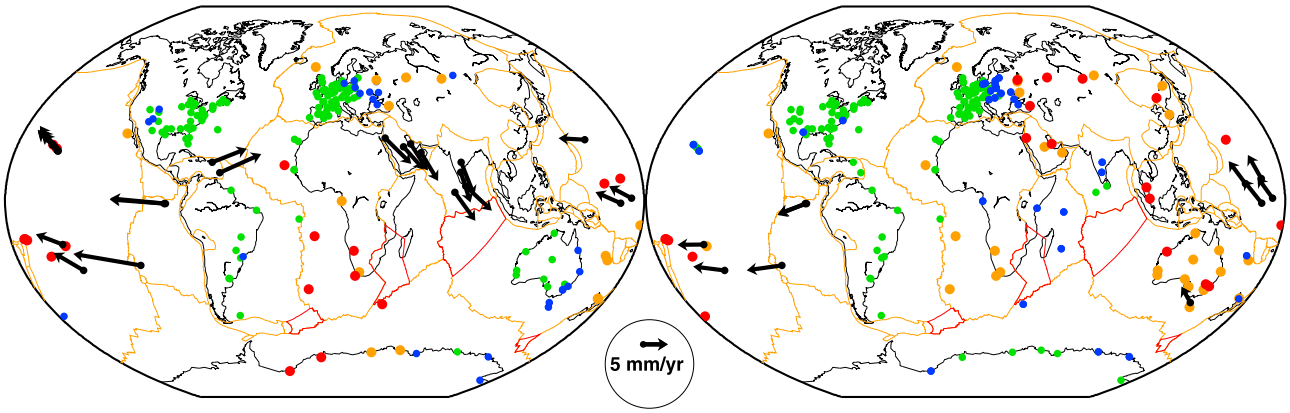

Figure 6. Velocity differences between ITRF2008 and (left) NNR-NUVEL-1A and (right) NNR-MORVEL56 after rotation rate transformation. Legend as in Figure 4.

all the 198 site velocities, yields large RMS: respectively 2.5 and 2.1 mm/a in east and north components. The 198 site velocity residuals are illustrated in Figure 6 (left). The large RMS values are due to, again, the large discrepancies between ITRF2008 and NNR1A for sites located on ARAB, CARB, INDI, NAZC and part of the PCFC plates.

[38] The large X-rotation rate of 0.083 mas/a found between ITRF2008 and NNRM56 is originated mostly from the rotation rate between the two geological models. If we consider a rotational alignment of future ITRF solutions to NNRM56, this will generate systematic ITRF velocity change up to 2.5 mm/a as well as an equivalent rate in its time evolution and the associated Earth Rotation Parameters. This change might be a drawback for some ITRF user applications, in which the ITRF rotation rate is purely conventional.

[39] Removing the NNRM56 rotation rates with respect to ITRF2008 from the entire set of 206 sites yields an RMS of the differences of respectively 1.8 and 1.9 mm/a for east and north components. The 206 site velocity residuals after this transformation are illustrated in Figure 6 (right). The smaller NNRM56 RMS values, compared to NNR1A (1.8 and 1.9 versus 2.5 and 2.0 mm/a) is an indication that NNRM56 is superior to NNR1A for ARAB, CARB, INDI, NAZC, NUBI, SOMA plates, and partly for PCFC plate (compare Figures 6 (left) and 6 (right)). However, comparing Figures 5 (right) and 6 (right), we clearly see that applying the estimated rotation rates between ITRF2008 and NNRM56 to the whole set of 206 sites reduces the velocity differences almost everywhere, except that it induces large residuals for all sites in Australia, the two sites on Sundaland and for the three sites on the Amurian plate. The Australia plate behavior here is very similar to the results of the comparison of the two geological models discussed above. It is probably not surprising that the Sundaland and Amurian site velocity residuals follow the Australia residual amplifications. In fact, according to *DeMets et al.* [2010], the two former plates were tied to MORVEL using GPS site velocities that were expressed in the Australia-fixed frame. However, the Caribbean plate is one of the six plates tied to MORVEL using GPS data and has its motion determined partly from GPS station velocities, expressed in the North America-fixed frame [*DeMets et al.*, 2010] and for which we observe a good agreement with ITRF2008-PMM at the level of 1–2 mm/a. This suggests that the amplification of Sundaland and Amurian residual velocities is not due to possible errors in GPS data used to tie these two plates to MORVEL.

6.3. Evaluation of the Uncertainty of the NNR Condition

[40] Although both geological models satisfy the NNR condition (but using distinct relative plate motions and sampling), comparing them via our selected network of sites shows a mean X-rotation rate between them of 0.058 mas/a (≈1.8 mm/a). Considering this number and the large X-rotation rate between ITRF2008 and NNRM56 (0.083 mas/a), we can conclude that the accuracy of the ITRF2008 NNR implicit realization may not be better than 2 mm/a. Given these results, and in particular the large NNR1A and NNRM56 differences, we will probably continue to operate, conventionally, successive orientation rate alignments of the future ITRF solutions. The internal consistency between ITRF solutions will be maintained with such a condition.

7. Conclusion

[41] We estimated a precise absolute plate motion model of 14 tectonic plates, involving velocities of 206 sites of high quality, extracted from and consistent with ITRF2008. Applying predictions based on Glacial Isostatic Adjustment model of *Schotman and Vermeersen* [2005] to site velocities improves the plate motion estimation in Eurasia, but degrades the fit in Antarctica and for a large part in North America. *Peltier*'s [2004] VM2 or VM4 GIA models partially improve the fit in Antarctica and Eurasia, but degrade the fit significantly in North America. Excluding 47 sites located in GIA regions, and not applying any GIA model corrections provide an estimated ITRF2008 plate motion model with a precision at the level of 0.3 mm/a WRMS.

[42] Estimating a translation rate vector together with plate angular velocities, allows quantifying the origin rate bias of the involved velocity field. Using our selection of 206 sites, we found a small origin rate bias, at the level of 0.4 ± 0.6 mm/a (95 per cent confidence limits), which could be considered as insignificant. Consequently, the resulting ITRF2008 plate motion model is consistent with ITRF2008 at the level of 0.4 mm/a, and is coherent with its precision of 0.3 mm/a WRMS. However, the users are advised to use the

Table A1. Sites and Their Horizontal Velocities Used in the Rotation Poles Estimation Together With Their One-Sigma Formal Errors and Post-Fit Residuals

							Horizontal Velocities (mm/a)				Residuals (mm/a)	
CODE	DOMES #	Site Name	Plate	T[a]	λ (deg)	ϕ (deg)	*Ve*	*Vn*	σVe	σVn	E	N
CHAN	21611M002	Changchun	Amurian	P	125.444	43.598	25.67	−11.74	0.13	0.15	0.36	0.63
TAEJ	23902M001	Taejon	Amurian	P	127.366	36.191	26.66	−12.56	0.06	0.06	0.02	0.01
KHAJ	12361M001	Khabarovsk	Amurian	P	135.046	48.330	22.22	−13.81	0.08	0.10	−0.21	−0.38
MARA	30313S001	Marion Island	Antarctica	D	37.857	−46.687	6.98	1.60	0.57	0.53	2.08	−1.61
SYOG	66006S002	Syowa	Antarctica	DPR	39.584	−68.878	−4.00	2.76	0.04	0.05	0.07	−0.04
MAW1	66004M001	Mawson Station	Antarctica	P	62.871	−67.469	−3.70	−2.31	0.04	0.05	−0.10	−0.15
DAV1	66010M001	Davis	Antarctica	P	77.973	−68.446	−2.79	−5.26	0.04	0.06	0.25	−0.03
CAS1	66011M001	Casey	Antarctica	P	110.520	−66.141	1.73	−9.99	0.04	0.05	−0.35	0.33
DUM1	91501M001	Ile des Petrels	Antarctica	DP	140.002	−66.525	8.36	−11.42	0.06	0.08	0.92	0.71
MCM4	66001M003	Mc Murdo	Antarctica	P	166.669	−77.759	9.95	−11.57	0.04	0.05	0.76	−0.47
BELB	66018S001	Belgrano	Antarctica	D	325.372	−77.795	2.46	12.09	0.88	0.90	−1.07	−0.28
VESL	66009M001	Sanae	Antarctica	P	357.158	−71.559	−0.55	10.37	0.04	0.05	−0.14	0.18
HALY	20102M001	Halat Ammar	Arabia	P	36.100	28.976	27.12	23.01	0.27	0.24	1.12	−0.34
7832	20101S001	Solar Village	Arabia	L	46.400	24.764	31.84	28.95	0.14	0.13	0.55	0.72
BHR2	24901M002	Bahrein (Juffar)	Arabia	P	50.608	26.057	31.14	30.03	0.06	0.06	−0.10	0.10
YIBL	25001M001	Yibal/Oman	Arabia	P	56.112	22.052	35.20	31.87	0.12	0.10	0.16	−0.12
YAR1	50107M004	Yarragadee	Australia	DLP	115.347	−28.884	38.96	57.79	0.05	0.06	−0.01	−0.08
NNOR	50181M001	New Norcia	Australia	P	116.193	−30.879	38.66	58.08	0.07	0.08	0.41	0.04
KARR	50139M001	Karratha	Australia	P	117.097	−20.853	38.89	58.36	0.06	0.05	−0.06	0.08
DARW	50134M001	Darwin	Australia	P	131.133	−12.761	35.62	59.38	0.08	0.05	−0.23	0.14
CEDU	50138M001	Ceduna	Australia	P	133.810	−31.694	29.11	58.70	0.06	0.06	0.44	−0.19
ALIC	50137M001	Alice Springs	Australia	P	133.886	−23.529	32.01	59.10	0.06	0.05	0.09	0.15
ADE1	50109S001	Salisbury	Australia	P	138.647	−34.549	24.76	58.46	0.06	0.06	0.15	0.34
BUR1	50144M001	Burnie	Australia	P	145.915	−40.860	15.54	57.29	0.18	0.22	−0.84	1.12
TOW2	50140M001	Townsville	Australia	P	147.056	−19.150	28.84	55.87	0.06	0.05	−0.29	−0.14
HOB2	50116M004	Hobart	Australia	PR	147.439	−42.613	14.12	55.80	0.06	0.07	−0.07	0.16
PARK	50108M001	Parkes	Australia	PR	148.265	−32.823	19.40	55.05	0.20	0.21	−0.99	−0.41
TIDB	50103M108	Tidbinbilla	Australia	DLPR	148.980	−35.218	18.23	55.49	0.06	0.07	−0.17	0.32
STR1	50119M002	Mount Stromlo	Australia	DLP	149.010	−35.134	18.40	55.52	0.06	0.07	−0.03	0.36
SYDN	50124M003	Sydney	Australia	P	151.150	−33.603	17.99	54.60	0.12	0.14	−0.37	0.26
SUNM	50143M001	Brisbane	Australia	P	153.035	−27.328	21.57	53.65	0.20	0.22	−0.29	0.04
KOUC	92727S001	Koumac	Australia	P	164.287	−20.432	24.15	47.81	0.08	0.10	1.10	0.07
NOUM	92701M003	Noumea	Australia	DP	166.410	−22.135	20.52	46.12	0.07	0.09	−0.52	−0.28
TAKL	50216S001	Auckland T. Gauge	Australia	P	174.770	−36.659	4.98	40.01	0.13	0.23	0.45	−0.38
AUCK	50209M001	Auckland	Australia	P	174.834	−36.419	4.51	39.88	0.04	0.07	−0.23	−0.46
CRO1	43201M001	Sainte Croix	Caribbean	PR	295.416	17.645	10.59	13.44	0.07	0.06	−0.03	−0.04
BARB	43401S001	Bridgetown	Caribbean	P	300.391	13.003	13.98	16.09	0.27	0.15	0.21	−0.04
HERS	13212M007	Herstmonceux	Eurasia	LP	0.336	50.679	16.80	16.57	0.04	0.07	−0.15	0.16
EBRE	13410M001	Roquetes	Eurasia	P	0.492	40.631	19.62	16.31	0.05	0.14	0.05	−0.20
SHEE	13236M001	Sheerness	Eurasia	P	0.743	51.258	17.04	16.13	0.06	0.10	0.17	−0.26
BELL	13431M001	Bellmunt	Eurasia	P	1.401	41.409	19.08	15.91	0.17	0.47	−0.48	−0.55
TOUL	10003M004	Toulouse	Eurasia	DP	1.481	43.369	19.54	16.23	0.04	0.09	0.43	−0.20
OPMT	10001S006	Paris	Eurasia	P	2.335	48.645	18.32	15.93	0.04	0.11	0.39	−0.40
MALL	13444M001	Palma de Mallorc	Eurasia	P	2.625	39.364	19.08	16.33	0.18	0.30	−1.15	−0.09
BRUS	13101M004	Brussels	Eurasia	P	4.359	50.609	17.51	16.07	0.04	0.07	−0.32	−0.11
SJDV	10090M001	Saint-Jean-des-v	Eurasia	P	4.677	45.687	19.53	15.96	0.04	0.08	0.36	−0.24
REDU	13102M001	Redu	Eurasia	P	5.145	49.812	18.24	15.75	0.06	0.16	0.02	−0.38
TERS	13534M001	Terschelling	Eurasia	P	5.219	53.178	18.15	14.77	0.30	0.84	0.84	−1.31
MARS	10073M008	Marseille	Eurasia	P	5.354	43.087	19.92	15.95	0.06	0.13	0.02	−0.23
EIJS	13533M001	Eijsden	Eurasia	P	5.684	50.570	17.86	16.03	0.32	0.91	−0.26	−0.04
KOSG	13504M003	Kootwijk	Eurasia	P	5.810	51.992	18.01	16.28	0.04	0.07	0.24	0.23
WSRT	13506M005	Westerbork	Eurasia	P	6.605	52.729	17.64	16.44	0.04	0.06	−0.10	0.46
BORK	14268M001	Borkum	Eurasia	P	6.747	53.380	17.97	15.69	0.10	0.14	0.39	−0.27
7203	14209S001	Effelsberg	Eurasia	R	6.884	50.336	18.40	16.03	0.09	0.25	−0.03	0.04
WAB2	14014M002	Wabern	Eurasia	P	7.464	46.732	19.80	16.02	0.05	0.12	0.34	0.04
ZIMM	14001M004	Zimmerwald	Eurasia	LP	7.465	46.685	19.68	16.32	0.04	0.07	0.21	0.34
IENG	12724S001	Torino	Eurasia	P	7.639	44.823	20.57	15.81	0.04	0.09	0.63	−0.18
HELG	14264M001	Helgoland Island	Eurasia	P	7.893	53.992	17.52	16.09	0.04	0.08	−0.14	0.23
AJAC	10077M005	Ajaccio	Eurasia	LP	8.763	41.736	21.06	15.97	0.04	0.08	0.26	0.05
PTBB	14234M001	Braunschweig	Eurasia	P	10.460	52.110	18.89	15.78	0.05	0.10	0.18	0.14
OBER	14208M001	Oberpfaffenhofen	Eurasia	P	11.280	47.895	20.29	15.85	0.05	0.09	0.36	0.24
WARN	14277M002	Warnemuende	Eurasia	P	12.101	53.987	17.93	15.31	0.22	0.29	−0.64	−0.14
BUDP	10101M003	Copenhagen	Eurasia	P	12.500	55.560	17.97	15.06	0.06	0.10	−0.26	−0.33
WTZR	14201M010	Wettzell	Eurasia	LPR	12.879	48.954	20.28	15.55	0.04	0.06	0.28	0.12
POTS	14106M003	Potsdam	Eurasia	LP	13.066	52.193	19.13	15.22	0.04	0.06	−0.10	−0.15
SASS	14281M001	Sassnitz	Eurasia	P	13.643	54.331	18.18	15.59	0.19	0.25	−0.63	0.30
GOPE	11502M002	Pecny - Ondrejov	Eurasia	P	14.786	49.724	20.21	15.03	0.05	0.11	0.02	−0.17
GRAZ	11001M002	Graz Lustbuehel	Eurasia	LP	15.493	46.875	21.79	15.67	0.05	0.08	0.83	0.52

Table A1. (continued)

CODE	DOMES #	Site Name	Plate	T[a]	λ (deg)	ϕ (deg)	Horizontal Velocities (mm/a)				Residuals (mm/a)	
							Ve	*Vn*	σVe	σVn	E	N
WROC	12217M001	Wroclaw	Eurasia	P	17.062	50.925	19.82	14.74	0.04	0.07	−0.52	−0.17
BOR1	12205M002	Borowiec	Eurasia	LP	17.073	52.091	20.03	14.85	0.04	0.07	−0.04	−0.04
PENC	11206M006	Penc	Eurasia	P	19.282	47.598	22.28	14.67	0.06	0.09	0.78	0.02
LAMA	12209M001	Lamkowko	Eurasia	P	20.670	53.709	20.22	14.39	0.05	0.07	−0.17	0.01
JOZE	12204M001	Jozefoslaw	Eurasia	P	21.032	51.911	21.07	14.44	0.05	0.07	0.18	0.08
BOGO	12207M002	Borowa gora	Eurasia	P	21.035	52.290	20.48	14.39	0.06	0.09	−0.32	0.04
KLPD	10802M001	Klaipeda	Eurasia	P	21.119	55.536	19.63	14.15	0.13	0.22	−0.40	−0.14
UZHL	12301M001	Uzhgorod	Eurasia	P	22.298	48.441	21.88	13.86	0.05	0.08	0.01	−0.34
SULP	12366M001	Lviv	Eurasia	P	24.014	49.646	21.70	14.08	0.06	0.09	−0.23	0.15
RIGA	12302M002	Riga	Eurasia	LP	24.059	56.772	20.25	13.37	0.06	0.09	−0.05	−0.47
GLSV	12356M001	Golosiiv - Kiev	Eurasia	P	30.497	50.175	22.36	12.91	0.05	0.06	−0.58	0.10
MIKL	12335M001	Nikolaiev	Eurasia	P	31.973	46.781	23.44	12.51	0.07	0.09	−0.34	−0.06
CRAO	12337M002	Simeiz	Eurasia	LPR	33.991	44.221	23.94	12.03	0.07	0.09	−0.53	−0.17
KHAR	12314M001	Kharkiv	Eurasia	P	36.239	49.816	23.49	11.71	0.27	0.36	−0.41	0.03
MOBN	12365M001	Obninsk/Moscow	Eurasia	P	36.570	54.934	23.11	12.03	0.07	0.09	0.15	0.47
ZWEN	12330M001	Zwenigorod	Eurasia	P	36.759	55.520	22.98	12.41	0.08	0.11	0.12	0.90
MDVO	12309M002	Mendeleevo	Eurasia	P	37.224	55.849	22.71	11.76	0.05	0.07	−0.16	0.35
ZECK	12351M001	Zelenchukskaya	Eurasia	PR	41.565	43.596	25.48	11.57	0.08	0.09	−0.06	0.95
ARTU	12362M001	Arti	Eurasia	P	58.560	56.252	25.01	6.22	0.05	0.06	−0.42	−0.08
NVSK	12319M001	Novossibirsk	Eurasia	P	83.235	54.659	27.04	−1.05	0.05	0.11	0.43	−0.46
KSTU	12349M002	Krasnoyarsk	Eurasia	DP	92.794	55.815	25.02	−4.41	0.07	0.18	−1.08	−1.11
CASC	13909S001	Cascais	Eurasia	P	350.581	38.506	17.84	16.82	0.04	0.08	−0.48	0.03
TORS	10108S001	Hvitanes	Eurasia	P	353.235	61.864	10.30	17.47	0.12	0.22	−1.42	0.95
NEWL	13273M103	Bartinney	Eurasia	P	354.457	49.914	15.68	16.64	0.06	0.10	−0.23	0.02
BRST	10004M004	Brest	Eurasia	P	355.503	48.189	16.22	17.18	0.05	0.10	−0.41	0.57
MADR	13407S012	Madrid-Robledo	Eurasia	PR	355.750	40.239	18.69	16.37	0.04	0.08	−0.11	−0.33
VILL	13406M001	Villafranca	Eurasia	P	356.048	40.254	19.42	16.74	0.04	0.09	0.56	0.06
CANT	13438M001	Cantabria	Eurasia	P	356.202	43.280	18.71	16.67	0.08	0.17	0.59	0.02
YEBE	13420M001	Yebes	Eurasia	PR	356.911	40.335	18.89	16.42	0.04	0.08	−0.10	−0.25
ABER	13231M001	Aberdeen	Eurasia	P	357.920	56.968	14.88	15.78	0.06	0.11	0.37	−0.67
MORP	13299S001	Morpeth	Eurasia	P	358.315	55.032	15.47	16.08	0.04	0.08	0.26	−0.37
NSTG	13216M001	North Shields	Eurasia	P	358.560	54.826	16.10	16.19	0.15	0.24	0.77	−0.26
HRM1	13235S001	Hermitage	Eurasia	P	358.716	51.266	16.56	16.54	0.04	0.07	0.12	0.06
LROC	10023M001	La Rochelle	Eurasia	P	358.781	45.967	18.14	16.34	0.04	0.10	0.21	−0.19
ALAC	13433M001	Alicante	Eurasia	P	359.519	38.152	19.86	16.64	0.04	0.09	−0.08	0.05
CHIZ	10020M001	Chize	Eurasia	P	359.592	45.941	18.67	16.33	0.10	0.15	0.58	−0.17
NPLD	13234M003	Teddington	Eurasia	P	359.660	51.233	16.99	16.09	0.05	0.11	0.35	−0.34
VALE	13439M001	Valencia	Eurasia	P	359.662	39.292	20.10	16.33	0.09	0.17	0.38	−0.24
MALD	22901S001	Male Airport	India	DP	73.526	4.161	46.58	35.17	0.08	0.06	0.85	0.90
IISC	22306M002	Bangalore	India	P	77.570	12.937	41.84	35.51	0.05	0.05	−0.34	−0.02
HYDE	22307M001	Hyderabad	India	P	78.551	17.308	40.88	34.94	0.09	0.12	0.76	−0.85
COLA	23501S001	Colombo	India	D	79.874	6.846	47.43	36.96	2.06	1.00	2.42	0.71
PUC1	49750S001	Price/Carbon	N. America	P	249.191	39.410	−14.02	−8.19	0.06	0.10	−0.05	−0.47
PIE1	40456M001	Pietown	N. America	PR	251.881	34.123	−13.47	−6.64	0.06	0.08	−0.52	0.21
7611	40463S001	Los Alamos	N. America	R	253.754	35.593	−13.81	−5.92	0.05	0.07	−0.38	0.31
NISU	49507M001	Boulder	N. America	P	254.738	39.806	−14.83	−5.60	0.12	0.22	−0.35	0.30
AMC2	40472S004	Colorado Springs	N. America	P	255.475	38.615	−14.39	−5.60	0.05	0.08	−0.13	0.05
MDO1	40442M012	Fort Davis	N. America	LPR	255.985	30.512	−12.10	−5.54	0.05	0.07	0.16	−0.06
SUM1	49743S001	Summerfield	N. America	P	257.488	34.645	−13.12	−5.43	0.08	0.14	0.28	−0.46
AUS5	49579S002	Austin	N. America	P	262.244	30.144	−10.84	−3.71	0.29	0.60	1.56	−0.38
PATT	49876S001	Palestine	N. America	P	264.281	31.606	−12.77	−2.67	0.18	0.43	0.09	−0.05
ANG1	49569S001	Angleton	N. America	P	264.515	29.138	−12.85	−3.13	0.13	0.30	−0.68	−0.61
WNFL	49488M001	Winnfield	N. America	P	267.218	31.725	−12.47	−1.85	0.20	0.71	0.47	−0.26
NLIB	40465M001	North Liberty	N. America	PR	268.425	41.580	−15.51	−1.22	0.04	0.07	−0.06	−0.04
MIL1	49862S001	Milwaukee	N. America	P	272.112	42.811	−15.74	−0.25	0.17	0.49	0.02	−0.37
MLF1	49484M001	Millers Ferry	N. America	P	272.608	31.917	−12.37	1.15	0.05	0.12	0.66	0.84
STB1	49861S001	Sturgeon Bay	N. America	P	272.686	44.603	−16.88	0.13	0.17	0.52	−0.73	−0.19
UNIV	49624S001	Jackson	N. America	P	275.614	42.094	−15.27	1.12	0.06	0.14	0.29	−0.23
LEBA	49631S001	Lebanon, Ohio	N. America	P	275.717	39.242	−14.68	1.58	0.07	0.18	0.22	0.18
BAYR	49612S001	Saginaw	N. America	P	276.108	43.254	−15.81	0.92	0.05	0.13	0.02	−0.61
MCN1	49479M001	Macon	N. America	P	276.439	32.521	−12.78	1.62	0.06	0.14	0.38	−0.05
ASHV	49853S001	Asheville	N. America	P	277.454	35.418	−14.00	2.03	0.06	0.14	−0.09	0.01
MCD1	49778S001	Mac Dill	N. America	P	277.468	27.691	−10.77	1.44	0.09	0.17	1.02	−0.60
SAV1	49474M001	Savannah	N. America	P	278.304	31.965	−12.75	2.37	0.14	0.28	0.22	0.05
CCV3	40426M002	Cap Canaveral	N. America	P	279.455	28.299	−12.13	2.67	0.07	0.12	−0.20	−0.06
7219	40499S001	Wrightwood	N. America	P	279.615	25.464	−9.71	2.57	0.11	0.17	1.39	−0.23
CHA1	49851S001	Charleston	N. America	P	280.157	32.583	−12.82	2.72	0.06	0.11	0.28	−0.25
7204	40441S001	Greenbank	N. America	R	280.164	38.251	−14.32	3.10	0.09	0.19	0.24	0.13
PSU1	49466M001	Penn State	N. America	P	282.150	40.617	−15.22	3.92	0.05	0.08	−0.16	0.27

Table A1. (continued)

CODE	DOMES #	Site Name	Plate	T[a]	λ (deg)	ϕ (deg)	Horizontal Velocities (mm/a)				Residuals (mm/a)	
							Ve	*Vn*	σVe	σVn	E	N
GODE	40451M123	Washington	N. America	DLPR	283.173	38.834	−14.62	4.02	0.04	0.06	−0.03	0.01
GLPT	49467M001	Gloucester Point	N. America	P	283.501	37.063	−14.17	4.11	0.05	0.08	−0.02	−0.02
USNA	49908S001	Annapolis	N. America	P	283.521	38.795	−14.53	3.47	0.05	0.08	0.04	−0.67
SOL1	49907S001	Solomons Island	N. America	P	283.546	38.132	−14.45	4.15	0.04	0.07	−0.04	0.01
HNPT	49913S001	Horn point	N. America	P	283.870	38.401	−14.67	3.56	0.04	0.07	−0.22	−0.69
DUCK	49846S001	Kitty hawk	N. America	P	284.249	35.999	−12.60	4.78	0.09	0.15	1.25	0.39
VIMS	49880S001	Wachapreague	N. America	P	284.313	37.422	−14.26	4.52	0.19	0.36	−0.06	0.11
DNRC	49470M001	Dover, Delaware	N. America	P	284.476	38.972	−15.30	4.13	0.11	0.19	−0.73	−0.33
CHL1	49845S001	Cape Henlopen	N. America	P	284.912	38.589	−14.16	4.35	0.23	0.44	0.30	−0.27
7618	40471S001	Hancock	N. America	R	288.013	42.742	−15.24	5.36	0.06	0.09	−0.01	−0.31
WES2	40440S020	Westford	N. America	PR	288.507	42.422	−15.15	5.51	0.05	0.07	−0.02	−0.32
NPRI	49684S001	Newport, Rhode i	N. America	P	288.672	41.319	−15.00	5.62	0.06	0.09	−0.13	−0.27
BARH	49927S001	Bar Harbor	N. America	P	291.778	44.203	−15.32	6.78	0.05	0.08	−0.05	−0.14
EPRT	49928S001	Eastport	N. America	P	293.008	44.716	−15.41	7.22	0.07	0.10	−0.14	−0.11
UNB1	40146S001	Fredericton	N. America	P	293.358	45.758	−15.99	7.28	0.10	0.16	−0.56	−0.16
BRMU	42501S004	Bermuda	N. America	P	295.304	32.197	−11.92	8.60	0.06	0.07	0.33	0.46
HLFX	40120M001	Halifax	N. America	P	296.389	44.491	−15.12	8.55	0.06	0.08	−0.21	0.12
EISL	41703M003	Easter Island	Nazca	LP	250.617	−26.992	67.23	−6.01	0.06	0.08	0.12	0.08
GALA	42005M001	Santa Cruz	Nazca	P	269.696	−0.738	51.24	10.27	0.04	0.04	−0.03	−0.08
GALA	42004S001	San Cristobal	Nazca	D	270.384	−0.895	51.27	11.16	0.55	0.26	−0.13	0.23
NKLG	32809M002	Libreville	Nubia	DP	9.672	0.352	22.23	19.09	0.04	0.04	−0.26	−0.05
WIND	31101M001	Windhoek	Nubia	P	17.089	−22.439	18.86	20.00	0.11	0.13	−0.86	0.91
SIMO	30307M001	Simonstown	Nubia	P	18.440	−34.009	16.52	19.68	0.06	0.08	−0.35	0.63
SUTH	30314M002	Sutherland	Nubia	P	20.810	−32.206	17.06	19.10	0.06	0.08	0.16	0.18
SALB	39601S002	Palmeira	Nubia	P	337.065	16.626	16.57	14.68	1.03	0.57	−2.36	−1.52
LPAL	81701M001	La Palma	Nubia	P	342.106	28.602	16.14	16.63	0.12	0.16	0.26	−0.27
DAKA	34106M001	Dakar University	Nubia	P	342.535	14.590	20.29	16.60	0.18	0.16	0.45	−0.48
DAKA	34101S004	Dakar	Nubia	D	342.567	14.638	20.62	17.31	1.06	0.54	0.78	0.22
MAS1	31303M002	Maspalomas	Nubia	P	344.367	27.605	16.57	17.20	0.05	0.07	0.09	−0.02
GOUG	30608M001	Gough Island	Nubia	P	350.119	−40.159	21.19	18.82	0.05	0.10	−0.05	0.56
HELA	30606S002	Saint-Helena	Nubia	D	354.333	−15.841	23.38	16.57	0.94	0.54	0.34	−2.05
MCIL	21789S001	Minamitorishima	Pacific	P	153.979	24.146	−71.64	23.74	0.08	0.08	0.23	0.05
POHN	51601M001	Pohnpei	Pacific	P	158.210	6.914	−70.05	25.75	0.12	0.07	−0.37	0.27
NAUR	50701M001	Nauru	Pacific	P	166.926	−0.548	−68.24	29.48	0.09	0.06	−1.16	0.74
KWJ1	50506M001	Kwajalein Atoll	Pacific	P	167.730	8.665	−69.06	29.96	0.10	0.08	0.33	0.90
KIRI	50305M001	Betio Island	Pacific	P	172.923	1.346	−68.05	31.23	0.06	0.05	−0.45	0.58
TUVA	51101M001	Funafuti	Pacific	P	179.197	−8.469	−64.01	32.39	0.05	0.06	0.51	0.20
CHAT	50207M001	Chatham Island	Pacific	DP	183.434	−43.764	−40.54	33.10	0.04	0.07	0.51	0.42
FALE	50601S001	Faleolo Airport/	Pacific	P	188.000	−13.743	−64.11	33.29	0.05	0.06	−0.85	−0.49
SAMO	50603M001	Apia	Pacific	P	188.262	−13.760	−63.80	33.31	0.07	0.08	−0.51	−0.51
ASPA	50503S006	American Samoa	Pacific	P	189.278	−14.234	−63.55	34.06	0.05	0.06	−0.31	0.12
CKIS	50213M003	Rarotonga	Pacific	P	200.199	−21.072	−62.26	35.16	0.07	0.07	−0.04	0.51
KOK1	49896S001	Kokole Point	Pacific	P	200.242	21.850	−62.15	35.38	0.09	0.09	0.34	0.40
KOKB	40424M004	Kauai	Pacific	PR	200.335	21.992	−62.27	34.41	0.06	0.06	0.16	−0.58
LHUE	49980S001	Lihue, Kauai	Pacific	P	200.661	21.851	−61.78	34.81	0.09	0.09	0.63	−0.18
HNLC	49970S001	Honolulu	Pacific	P	202.135	21.173	−62.66	34.51	0.05	0.06	−0.30	−0.48
MAUI	40445S008	Maui	Pacific	LP	203.743	20.580	−61.93	34.61	0.05	0.05	0.36	−0.37
UPO1	49895S001	Upolu Point	Pacific	P	204.116	20.121	−61.95	34.74	0.07	0.07	0.42	−0.21
MKEA	40477M001	Mauna Kea	Pacific	PR	204.544	19.679	−62.68	34.89	0.06	0.05	−0.17	−0.08
HILO	49979S001	Hilo Airport	Pacific	P	204.947	19.597	−62.85	35.59	0.06	0.06	−0.43	0.66
7121	92202M002	Huahine	Pacific	LP	208.959	−16.628	−67.23	33.50	1.38	1.32	−1.84	−0.93
THTI	92201M009	Papeete (Tahiti)	Pacific	DLP	210.394	−17.467	−65.73	34.27	0.07	0.06	−0.31	−0.03
RAQB	92403S001	Rapa	Pacific	D	215.665	−27.461	−65.00	34.41	0.69	0.49	−1.83	0.86
GUAX	40512M001	Isla Guadalupe	Pacific	P	241.710	28.722	−47.08	24.98	0.26	0.27	0.69	−1.91
BUE2	41505S007	Buenos Aires	S. America	P	301.481	−34.394	−0.33	12.16	0.06	0.07	0.70	0.38
LPGS	41510M001	La Plata	S. America	P	302.068	−34.726	−0.93	11.95	0.06	0.06	0.13	0.13
LKTH	80601S001	Port Stanley	S. America	P	302.149	−51.511	0.51	12.31	0.16	0.21	−0.25	0.57
KOUR	97301M210	Kourou	S. America	DP	307.194	5.217	−5.24	12.16	0.10	0.05	−0.68	−0.05
UEPP	41611M001	Presidente Prude	S. America	P	308.591	−21.986	−2.76	13.15	0.13	0.10	0.12	0.87
PARA	41610M001	Curitiba	S. America	P	310.769	−25.299	−3.14	12.31	0.10	0.08	−0.32	−0.07
NEIA	41620M001	Cananeia	S. America	P	312.075	−24.873	−1.57	13.76	0.43	0.33	1.40	1.32
BRAZ	41606M001	Brasilia	S. America	P	312.122	−15.846	−3.76	12.56	0.07	0.05	−0.22	0.10
FORT	41602M001	Forteleza	S. America	PR	321.574	−3.852	−4.68	12.42	0.10	0.05	−0.37	−0.21
ASC1	30602M001	Ascension	S. America	DP	345.588	−7.899	−5.58	11.08	0.05	0.05	−0.52	−0.57
MALI	33201M001	Malindi	Somalia	P	40.194	−2.976	26.37	16.71	0.09	0.04	−0.35	0.29
SEY1	39801M001	Mahe Island	Somalia	DP	55.479	−4.643	25.70	11.27	0.10	0.05	−0.08	−0.18
REUN	97401M003	La Reunion	Somalia	DP	55.572	−21.079	18.62	11.59	0.09	0.07	0.30	0.09
GETI	22703M001	Kota Bharu	Sunda	P	102.105	6.185	32.27	−4.84	0.33	0.23	−0.56	−0.18
NTUS	22601M001	Singapore	Sunda	P	103.680	1.337	30.38	−5.45	0.06	0.05	−0.03	0.04

Table A1. (continued)

CODE	DOMES #	Site Name	Plate	T[a]	λ (deg)	φ (deg)	Horizontal Velocities (mm/a)				Residuals (mm/a)	
							Ve	*Vn*	σ*Ve*	σ*Vn*	E	N
Rejected Points With Residuals Larger Than 3-sigma-3 mm												
CROB	91301S001	Ile de la Posses	Antarctica	D	51.856	−46.240	7.91	−1.03	1.40	1.23	3.11	−1.26
KERG	91201M002	Kerguelen	Antarctica	DP	70.256	−49.161	4.91	−2.44	0.04	0.07	0.42	1.06
HIL1	50141S001	Hillarys/Perth	Australia	P	115.739	−31.653	40.89	57.32	0.15	0.16	2.54	−0.77
PERT	50133M001	Perth	Australia	P	115.885	−31.630	39.25	57.78	0.06	0.07	0.95	−0.34
JAB1	50136M001	Jabiru	Australia	P	132.894	−12.577	34.82	60.69	0.13	0.07	−0.64	1.33
MOBS	50182M001	Melbourne Observ	Australia	P	144.975	−37.643	19.71	57.83	0.07	0.08	0.57	1.16
CREU	13432M001	Cap de Creus	Eurasia	P	3.316	42.127	23.04	20.70	0.24	0.67	3.15	4.39
BUCU	11401M001	Bucharest	Eurasia	P	26.126	44.272	23.23	12.40	0.05	0.07	−0.01	−1.25
POLV	12336M001	Poltava	Eurasia	P	34.543	49.413	22.43	12.56	0.05	0.07	−1.21	0.50
NOVJ	12367M001	Novosibirsk	Eurasia	P	82.909	54.849	23.91	0.55	0.07	0.16	−2.44	0.58
NRIL	12364M001	Norilsk	Eurasia	P	88.360	69.235	22.04	−1.98	0.04	0.05	−1.08	−0.03
YAKA	12353M001	Yakutsk	Eurasia	P	129.681	61.871	21.37	−9.81	0.11	0.15	0.88	2.15
ACOR	13434M001	A Coruna	Eurasia	P	351.601	43.172	21.28	16.27	0.04	0.09	3.77	−0.40
BILI	12363M001	Bilibino	N. America	P	166.438	67.943	8.72	−20.77	0.04	0.06	3.08	−0.88
AZCN	49504M001	Aztec, New Mexico	N. America	P	252.089	36.655	−14.29	−5.85	0.05	0.08	−0.80	1.18
VCIO	49490M001	Vici - Oklahoma	N. America	P	260.783	35.889	−12.96	−2.62	0.04	0.08	0.65	1.65
ARP3	49878S003	Aransas Pass	N. America	P	262.941	27.680	−13.94	−3.44	0.07	0.12	−2.68	−0.07
MEM2	49867S002	French Bayou	N. America	P	269.794	35.284	−15.76	−0.77	0.05	0.14	−1.86	0.01
SAG1	49475M001	Saginaw	N. America	P	276.162	43.436	−17.71	0.02	0.05	0.13	−1.74	−1.46
KYW1	49852S001	Key West Naval	N. America	P	278.347	24.437	−9.69	2.37	0.05	0.08	0.99	0.05
AOML	49914S001	Virginia Key	N. America	P	279.838	25.584	−9.91	2.57	0.05	0.08	1.02	−0.27
SHK1	49473M001	Sandy Hook	N. America	P	285.988	40.282	−11.92	5.02	0.24	0.45	3.09	−0.07
STJO	40101M001	St John's	N. America	PR	307.322	47.404	−14.84	12.88	0.05	0.06	−0.59	0.83
ARMA	33710S002	Arlit	Nubia	D	7.359	18.665	23.97	15.93	3.65	1.87	3.08	−3.36
MSKU	32810M001	Masuku	Nubia	P	13.552	−1.621	17.04	21.05	0.24	0.13	−5.17	1.58
TRIA	30604S001	Tristan da Cunha	Nubia	D	347.687	−36.880	24.29	21.94	0.92	0.66	2.29	3.73
4968	50505S003	Kwajalein Atoll	Pacific	R	167.482	9.337	−73.06	27.37	2.41	2.98	−3.55	−1.92
CACB	41609S001	Cachoeira Paulis	S. America	P	314.998	−22.546	0.51	11.79	0.70	0.48	3.84	−1.12
BINT	22702M001	Bintulu	Sunda	P	113.067	3.240	27.61	−10.20	0.87	0.45	−3.53	−0.65

[a]IERS Space Geodesy Technique Abbreviation: D for DORIS, L for SLR, P for GPS and R for VLBI.

complete ITRF2008-PMM parameters: the plate angular velocities (Table 3) and the translation rate components (Table 2).

[43] Comparing the two geological models, NNR-NUVEL-1A and NNR-MORVEL56, using 165 sites extracted from our selection of 206 sites, we found a large X-rotation rate of 0.058 mas/a, equivalent to a horizontal velocity of 1.8 mm/a at the equator. While this rotation rate, once removed, reduces the velocity differences between the two models for Eurasia, North America, Nubia, South America and part of the Pacific plate, the velocity residuals of all sites located on the Australia plate are amplified by at least 1 mm/a, reaching 4.6 mm/a.

[44] Using our selection of 206 sites as reference and after removing estimated rotation rates between ITRF2008 and both models, we found better agreement with NNR-MORVEL56 than with NNR-NUVEL-1A (compare Figures 6 (left) and 6 (right)) for Arabian, Antarctica, Caribbean, India, Nazca, Nubia and Somalia plates, as well as part of the Pacific plate. Both models perform equally in Eurasia, North and South Americas. However, we observe large velocity residuals between ITRF2008 and NNR-MORVEL56 for all sites on Australia plate (up to 4 mm/a, except for two sites: one in Auckland and one in New Caledonia), the two sites on Sundaland (up to 4.9 mm/a) and the three sites on the Amurian plate (up to 4.5 mm/a). These two plates were actually tied to MORVEL [*DeMets et al.*, 2010] via GPS velocities expressed in the Australia-fixed frame.

[45] The small rotation rates found between ITRF2008 and NNR-NUVEL-1A is an indication that the implicit alignment of ITRF2008 to NNR-NUVEL-1A is satisfied at the level of or better than 1 mm/a. However, the large X-rotation rate between the two geological models and between NNR-MORVEL56 and ITRF2008 (0.083 mas/a ≈ 2.5 mm/a) suggest that the accuracy of the NNR ITRF2008 implicit realization is not better than 2 mm/a. Considering the relatively large differences between the two geological models and the large X-rotation rates, and in order to ensure internal ITRF consistency, we probably will continue to operate rotation rate alignment between future ITRF solutions.

Appendix A: Sites Considered in ITRF2008-PMM Estimation

[46] Table A1 lists the 206 sites and their horizontal velocities used in the rotation poles estimation together with their one-sigma formal errors and post-fit residuals. The table also lists the 29 rejected sites where the velocity residuals exceed the threshold of 3-sigma-3mm.

[47] **Acknowledgments.** The ITRF activities are funded by the Institut National de l'Information Géographique et Forestière (IGN), France, and partly by Centre National d'Etudes Spatiales (CNES). We are very thankful to D. Argus for providing NNR-MORVEL56 model and GEODVEL angular velocities. We acknowledge useful comments and suggestions provided by D. Argus and C. DeMets which improved the content of this article. We thank Olivier Jamet and Xiaoping Wu for useful discussions. Three GIA models have been downloaded from the Special Bureau for Loading website (http://www.sbl.statkart.no/projects/pgs/ [*van Dam et al.*, 2002]).

References

Altamimi, Z., C. Boucher, and L. Duhem (1993), The worldwide centimetric terrestrial reference frame and its associated velocity field, *Adv. Space Res.*, *13*(11), 151–160.

Altamimi, Z., P. Sillard, and C. Boucher (2002), ITRF2000: A new release of the International Terrestrial Reference Frame for Earth science applications, *J. Geophys. Res.*, *107*(B10), 2214, doi:10.1029/2001JB000561.

Altamimi, Z., P. Sillard, and C. Boucher (2003), The impact of a no-net-rotation condition on ITRF2000, *Geophys. Res. Lett.*, *30*(2), 1064, doi:10.1029/2002GL016279.

Altamimi, Z., X. Collilieux, J. Legrand, B. Garayt, and C. Boucher (2007), ITRF2005: A new release of the International Terrestrial Reference Frame based on time series of station positions and Earth Orientation Parameters, *J. Geophys. Res.*, *112*, B09401, doi:10.1029/2007JB004949.

Altamimi, Z., X. Collilieux, and L. Métivier (2011), ITRF2008: An improved solution of the International Terrestrial Reference Frame, *J. Geod.*, *85*(8), 457–473, doi:10.1007/s00190-011-0444-4.

Argus, D. F. (2007), Defining the translational velocity of the reference frame of Earth, *Geophys. J. Int.*, *169*, 830–838, doi:10.1111/j.1365-246X.2007.03344.x.

Argus, D. F., and R. G. Gordon (1991), No-net-rotation model of current plate velocities incorporating plate motion model NUVEL-1, *Geophys. Res. Lett.*, *18*, 2038–2042.

Argus, D. F., and R. G. Gordon (1996), Tests of the rigid-plate hypothesis and bounds on intraplate deformation using geodetic data from very long baseline interferometry, *J. Geophys. Res.*, *101*, 13,555–13,572.

Argus, D. F., and W. R. Peltier (2010), Constraining models of postglacial rebound using space geodesy: A detailed assessment of model ICE-5G (VM2) and its relatives, *Geophys. J. Int.*, *181*, 697–723, doi:10.1111/j.1365-246X.2010.04562.x.

Argus, D. F., R. G. Gordon, M. B. Heflin, C. Ma, R. J. Eanes, P. Willis, W. R. Peltier, and S. E. Owen (2010), The angular velocities of the plates and the velocity of Earth's centre from space geodesy, *Geophys. J. Int.*, *180*(3), 916–960, doi:10.1111/j.1365-246X.2009.04463.x.

Argus, D. F., R. G. Gordon, and C. DeMets (2011a), Geologically current motion of 56 plate relative to the no-net-rotation reference frame, *Geochem. Geophys. Geosyst.*, *12*, Q11001, doi:10.1029/2011GC003751.

Argus, D. F., G. Blewitt, W. R. Peltier, and C. Kreemer (2011b), Rise of the Ellsworth mountains and parts of the East Antarctic coast observed with GPS, *Geophys. Res. Lett.*, *38*, L16303, doi:10.1029/2011GL048025.

Bird, P. (2003), An updated digital model of plate boundaries, *Geochem. Geophys. Geosyst.*, *4*(3), 1027, doi:10.1029/2001GC000252.

Blewitt, G. (2003), Self-consistency in reference frames, geocenter definition, and surface loading of the solid Earth, *J. Geophys. Res.*, *108*(B2), 2103, doi:10.1029/2002JB002082.

Blewitt, G., and D. Lavallée (2002), Effect of annual signals on geodetic velocity, *J. Geophys. Res.*, *107*(B7), 2145, doi:10.1029/2001JB000570.

Chambers, D. P., J. Wahr, M. E. Tamisea, and R. S. Nerem (2010), Ocean mass from GRACE and glacial isostatic adjustment, *J. Geophys. Res.*, *115*, B11415, doi:10.1029/2010JB007530.

Collilieux, X., and G. Woppelmann (2010), Global sea level rise and its relation to the terrestrial reference frame, *J. Geod.*, *85*(1), 9–22, doi:10.1007/s00190-010-0412-4.

DeMets, C., R. G. Gordon, D. F. Argus, and S. Stein (1990), Current plate motions, *J. Geophys. Res.*, *101*, 425–478.

DeMets, C., R. G. Gordon, D. F. Argus, and S. Stein (1994), Effect of recent revisions of the geomagnetic reversal timescale on estimates of current plate motions, *Geophys. Res. Lett.*, *21*(20), 2191–2194.

DeMets, C., R. G. Gordon, and D. F. Argus (2010), Geologically current plate motions, *Geophys. J. Int.*, *181*(1), 1–80, doi:10.1111/j.1365-246X.2009.04491.x.

Drewes, H. (1998), Combination of VLBI, SLR and GPS determined station velocities for actual plate kinematic and crustal deformation models, in *Geodesy on the Move: Gravity, Geoid, Geodynamics and Antarctica*, *IAG Symp.*, vol. 119, edited by R. Forsberg, M. Feissel, and R. Dietrich (ed.), pp. 377–382, Springer, Berlin.

Greff-Lefftz, M., L. Métivier, and J. Besse (2010), Dynamic mantle density heterogeneities and global geodetic observables, *Geophys. J. Int.*, *180*, 1080–1094, doi:10.1111/j.1365-246X.2009.04490.x.

Kierulf, H. P., H.-P. Plag, and O. Kristiansen (2003), Towards the true rotation of a rigid Eurasia, in *EUREF Publication*, vol. 12, edited by J. A. Torres and H. Hornik, pp. 118–124, Bundesamtes für Kartogr. und Geod., Frankfurt, Germany.

King, M., et al. (2010), Improved constraints on models of glacial isostatic adjustment. A review of the contribution of ground-based geodetic observations, *Surv. Geophys.*, *31*(5), 465–507, doi:10.1007/s10712-010-9100-4.

Kogan, M. G., and G. M. Steblov (2008), Current global plate kinematics from GPS (1995–2007) with the plate-consistent reference frame, *J. Geophys. Res.*, *113*, B04416, doi:10.1029/2007JB005353.

Kreemer, C., W. E. Holt, and A. J. Haines (2003), An integrated global model of present-day plate motions and plate boundary deformation, *Geophys. J. Int.*, *154*, 8–34.

Kreemer, C., D. A. Lavallee, G. Blewitt, and W. E. Holt (2006), On the stability of a geodetic no-net-rotation frame and its implication for the International Terrestrial Reference Frame, *Geophys. Res. Lett.*, *33*, L17306, doi:10.1029/2006GL027058.

Legrand, J. (2007), Champ de vitesses de l'ITRF, propriétés cinématiques de la croûte terrestre et condition de non rotation globale, PhD thesis, Obs. de Paris, Paris.

Métivier, L., M. Greff-Lefftz, and Z. Altamimi (2010), On secular geocenter motion: The impact of climate changes, *Earth Planet. Sci. Lett.*, *3–4*, 360–366, doi:10.1016/j.epsl.2010.05.021.

Métivier, L., X. Collilieux, and Z. Altamimi (2012), ITRF2008 contribution to glacial isostatic adjustment and recent ice melting assessment, *Geophys. Res. Lett.*, *39*, L01309, doi:10.1029/2011GL049942.

Minster, J. B., and T. H. Jordan (1978), Present-day plate motions, *J. Geophys. Res.*, *83*, 5331–5354.

Paulson, A., S. Zhong, and J. Wahr (2007), Limitations on the inversion for mantle viscosity from postglacial rebound, *Geophys. J. Int.*, *168*, 1195–1209, doi:10.1111/j.1365-246X.2006.03222.x.

Peltier, W. R. (2004), Global glacial isostasy and the surface of the ice-age Earth: The ICE-5G (VM2) model and GRACE, *Annu. Rev. Earth Planet. Sci.*, *32*, 111–149, doi:10.1146/annurev.earth.32.082503.144359.

Petit, G., and B. Luzum (Eds.) (2010), IERS conventions (2010), *IERS Tech. Note*, *36*, Bundesamts für Kartogr. und Geod., Frankfurt, Germany. [Available at http://tai.bipm.org/iers/conv2010/]

Plag, H. P., T. Norbech, and O. Kristiansen (2002), Effects on intraplate deformations on fixing regional reference frames, in *EUREF Publication*, vol. 10, edited by J. A. Torres and H. Hornik, pp. 118–124, Bundesamtes für Kartogr. und Geod., Frankfurt, Germany.

Schotman, H. H. A., and L. L. A. Vermeersen (2005), Sensitivity of glacial isostatic adjustment models with shallow low-viscosity Earth layers to the ice-load history in relation to the performance of GOCE and GRACE, *Earth Planet. Sci. Lett.*, *236*, 828–844.

van Dam, T., H.-P. Plag, O. Francis, and P. Gegout (2002), GGFC Special Bureau for Loading: Current status and plans, paper presented at IERS GGFC Workshop, Global Geophys. Fluids Cent., Int. Earth Rotation and Ref. Syst. Serv., Munich, Germany.

Wu, X., X. Collilieux, Z. Altamimi, B. L. A. Vermeersen, R. S. Gross, and I. Fukumori (2011), Accuracy of the International Terrestrial Reference Frame origin and Earth expansion, *Geophys. Res. Lett.*, *38*, L13304, doi:10.1029/2011GL047450.